



1  
2 **Permafrost changes in the northwestern Da Xing'anling Mountains, Northeast**  
3 **China in the past decade**

4 **Xiaoli Chang<sup>1,2\*</sup>, Huijun Jin<sup>2,3\*</sup>, Ruixia He<sup>2\*</sup>, Yanlin Zhang<sup>1</sup>, Xiaoying Li<sup>4</sup>, Xiaoying Jin<sup>2</sup>**  
5 **and Guoyu Li<sup>2</sup>**

6 <sup>1</sup> School of Earth Science and Spatial Information Engineering, Hunan University of Science and Technology,  
7 Xiangtan, Hunan 411201, China,

8 <sup>2</sup> State Key Laboratory of Frozen Soils Engineering, Northwest Institute of Eco-Environment and Resources, Chinese  
9 Academy of Sciences, Lanzhou 730000, China,

10 <sup>3</sup> School of Civil Engineering, Institute of Cold-Regions Science and Engineering, and Northeast-China Observatory  
11 and Research-Station of Permafrost Geo-Environment (Ministry of Education), Northeast Forestry University,  
12 Harbin 150040, China,

13 <sup>4</sup> Key Laboratory of Sustainable Forest Ecosystem Management (Ministry of Education) and College of Forestry,  
14 Northeast Forestry University, Harbin 150040, China

15 \*These authors contributed equally to this work.

16 \*Correspondence: R. He: ruixiahe@lzb.ac.cn

17

18 **Abstract**

19 Under a pronounced climate warming, permafrost has been degrading in most areas, but it is still  
20 unclear in the northwestern part of the Da Xing'anling Mountains, Northeast China. According to a  
21 ten-year observation of permafrost and active-layer temperatures, the multi-year average of mean  
22 annual ground temperatures at 20 m was  $-2.83$ ,  $-0.94$ ,  $-0.80$ ,  $-0.70$ ,  $-0.60$  and  $-0.49$  °C,  
23 respectively, at Boreholes GH4, MG3, MG1, MG2, GH5 and YTLH2, with the depths of permafrost  
24 table varying from 1.1 to 7.0 m. Ground cooling at shallow depths has been detected, resulting in  
25 declining thaw depths in Yituli'he during 2009-2020, possibly due to relatively stable mean positive  
26 air temperature and declining snow cover and dwindling local population. In most study areas (e.g.,  
27 Mangui and Genhe), permafrost warming is particularly pronounced at larger depths (even at 80 m).  
28 These results can provide important information for regional development and engineering design  
29 and maintenance.

30 **Key words:** Permafrost change, climate warming, ground warming and cooling, declined snow  
31 cover, dwindling local population

32 **Introduction**

33 Permafrost, defined as ground that remains at or below 0 °C consecutively for two or more years, is  
34 widespread in high-latitude and high-elevation regions (Zhang et al., 2007). One quarter of the  
35 Northern Hemisphere and 17% of the Earth's currently exposed land surface are underlain by  
36 permafrost (Biskaborn et al., 2019). Areal extent of permafrost in China is estimated at about  $1.59$   
37  $\times 10^6$  km<sup>2</sup> (Youhua et al., 2012), accounting for one-sixth of the total Chinese land territories. In



38 northeastern China, land area of about  $3.1 \times 10^5$  km<sup>2</sup> is underlain by permafrost (Zhang et al., 2021).  
39 Northern part of Northeast China is also characterized by the extensive and stable inversion of air  
40 temperature in winter, thick surficial deposits, dense vegetation, extensive snow cover, and  
41 widespread distribution of wetlands in valley bottoms and lowlands, resulting in strong regional  
42 differentiations in permafrost features (Jin et al., 2007). Therefore, the latitudinal permafrost in  
43 Northeast China is referred to as the “Xing’an (Hinggan)-Baikal permafrost (XBP)” (Jin et al., 2007),  
44 a distinct type of ecosystem-dominated permafrost (Shur and Jorgenson, 2007).

45 Permafrost is sensitive to climate change (Farquharson et al., 2019; Sim et al., 2021; Zhang et al.,  
46 2019) and surface disturbances (Guo et al., 2018; Li et al., 2019; Li et al., 2021). Permafrost has  
47 experienced significant warming and widespread degradation during the last several decades (Jin et  
48 al., 2000; Jin et al., 2007; Shanshan Chen, 2020; Zhang et al., 2019; Jin et al., 2021). It has been  
49 evidenced by deeper seasonal thaw (Luo et al., 2018), thinning and warming permafrost (Gruber,  
50 2012; Jin et al., 2021; Jin et al., 2007; Romanovsky et al., 2010), and an areal reduction of permafrost  
51 in northeastern China (Li et al., 2021; Zhang et al., 2021). However, most of the regional or local  
52 investigations conducted for economic development, engineering design and construction, and  
53 environmental management, such as water supply, road construction or coalmining (Jin et al., 2007),  
54 would be terminated upon the project completion. Numerous local studies on permafrost changes  
55 have been carried out in recent years; however, most of them have been based on air and/or ground  
56 surface temperatures provided by weather stations, reanalysis data (Wei et al., 2011; Zhang et al.,  
57 2018; Zhang et al., 2021), or short-term ground thermal observations (He et al., 2021; Jin et al.,  
58 2007). Thus, it is hard to more accurately feature and evaluate the latest distribution and future  
59 changes of permafrost in Northeast China under the combined influences of warming climate and  
60 human activities (Serban et al., 2021).

61 Fortunately, similar to the Circumpolar Active Layer Monitoring (CALM) sites (Brown et al.,  
62 2000; Grebenets et al., 2021; Shiklomanov et al., 2012), or CALM-South sites (Guglielmin, 2006;  
63 Guglielmin et al., 2012; Hrbáček et al., 2021), since 2009, a less comprehensive observing system  
64 was gradually established at Gen’he, Yituli’he, and Mangui in the northwestern part of the Da  
65 Xing’anling Mountains, Northeast China. Periodical collection and calibration of data on the thermal  
66 regimes of soils in the active layer and permafrost at depths have been carried out in boreholes,  
67 generally reaching 20 m in depth and one of them, 80 m, in Gen’he, eastern Inner Mongolia,  
68 Northeast China. This thus presents an opportunity to observe the thermal characteristics of the XAP  
69 at depths and to understand and evaluate temporal changes in permafrost features in different  
70 landscapes under a warming climate. These results can provide important information for regional  
71 planning, development, and engineering design and maintenance in Northeast China.

72

## 73 Study area

74 The Gen’he Station of China Forest Ecological Research Network (CFERN), Yituli’he Permafrost  
75 Observatory (YPO), and Mangui Permafrost Station (MPS) are found in the discontinuous  
76 permafrost zone of Northeast China (Figure 1), where it is characterized by a cold temperate  
77 continental climate under the influences of alternating monsoons. Multi-year averages of mean  
78 annual air temperature (MAAT) were  $-4.0$  °C at Gen’he (1961–2020),  $-5.2$  °C at the YPO (1965–  
79 2005) and  $-5.8$  °C at the MPS (1996–2005). In the same periods, the multi-year average of annual



80 precipitation was 440 mm at Gen'he, 460 mm at the YPO, and 480 mm at the MPS. Annual  
81 precipitation falls concentratively in the form of summer rain, according to the chorographic record  
82 of Gen'he city. Snowfall (snow water equivalent, or SWE) accounts for about 12~20% of annual  
83 total precipitation. Stable snow cover usually starts to occur on the ground surface in the late October  
84 and generally disappears in the next April.

85 Vegetation differs slightly from site to site where Boreholes GH4, GH5, YTLH1, YTLH2, MG1,  
86 MG2 and MG3 are located (Figure 1 and Table 1). Borehole GH4 is in a larch (*Larix gmelinii*) forest,  
87 whereas Boreholes GH5, YTLH1, YTLH2 and MG2 are in sedge (*Carex tato*) meadows. The  
88 Borehole MG3 is in an open backyard, and Borehole MG1, in a birch (*Betula*) shrubland with sedges  
89 (*Carex tato*) as an understory. However, soil types are similar (brown coniferous forest soil).

90

91 Figure 1. Location of the study area and the distribution of borehole sites in the zones of frozen ground in the  
92 northern Da Xing'anling Mountains, Northeast China

93 Among the seven boreholes, Borehole YTLH1 of 8.15 m in depth was first installed for monitoring  
94 the hydrothermal dynamics of active layer and shallow permafrost at the end of 2008, with weekly  
95 manual measurement of soil temperatures since 2009. However, in order to monitor the permafrost  
96 temperature at the depth of zero annual amplitude (generally at 10-25 m in Northeast China), an  
97 additional borehole (YTLH2) was drilled to a depth of 20 m at a nearby site (10 m away from the  
98 YTLH1) with almost identical physical and vegetative conditions on the ground surface. The  
99 thermistor cables were permanently installed for manually monitoring ground temperatures since  
100 2010. Boreholes GH4, GH5, MG1, MG2 and MG3 have been monitored since the beginning of  
101 2012, but for different observational frequencies (Table 1). These thermistor cables were assembled  
102 by the State Key Laboratory of Frozen Soils Engineering (SKLFSE), Cold and Arid Regions  
103 Environmental and Engineering Research Institute (CAREERI; now renamed to the Northwest  
104 Institute of Eco-Environment and Resources, or NIEER), Chinese Academy of Sciences (CAS),  
105 Lanzhou, China, with an accuracy of  $\pm 0.05$  °C in the temperature range from  $-30$  to  $+30$  °C, and  
106  $\pm 0.1$  °C, from  $-45$  to  $-30$  °C and  $+30$  to  $+50$  °C.

107 For continuous observation, data for ground temperatures at the Borehole GH4 were  
108 automatically collected hourly by the Micrologger CR3000 (USA), whereas at other sites were  
109 manually measured with a multi-meter (Fluke 189®). Unfortunately, not all records for soil  
110 temperature are complete for all boreholes. For example, there were two hiatuses for the records of  
111 Borehole GH4 (2014-2016 and 2017-2019) due to the logger damage. Manual records from January  
112 to June in 2014 for other boreholes were lost in mailing. The measurement at MG3 was halted in  
113 2016 because of borehole damage and that at GH5 and YTLH2, in 2020, due to the outbreak of the  
114 COVID-19 virus and the ensued traffic control. The specifics are presented in Table 1.

115 Table 1. Characteristics and monitoring information of ground temperature boreholes in the  
116 northwestern part of Da Xing'anling Mountains, Northeastern China



117

### 118 **3 Results**

#### 119 **3.1 Ground temperatures in near-surface permafrost and active layer**

120 Ground temperatures of near-surface soil (e.g., at depths of 1 and 2 m) responds quickly to changes  
121 in air temperature, but the change patterns of ground temperatures show a reduction of amplitude  
122 with increasing depth in all these boreholes. In Boreholes GH4, MG3, YTLH1 and YTLH2,  
123 seasonal variations in ground temperature still could be detected at the depth of 5 m. However, at  
124 depths of 3 and 4 m, variations in winter ground temperatures gradually flattens out in Boreholes  
125 GH5, MG1 and MG2, and only the annual variability in summer ground temperatures can be  
126 detected at the depth of 5 m (Figure 2). Therefore, only a small temperature amplitude (0.5~1.0°C)  
127 was detected at the depth of 5 m in comparison with that at 3 m (2~3°C).

128

129 Figure 2. Variability of measured ground temperatures at depths of 1-5 m for Boreholes GH4 and GH5  
130 (a)), MG1, MG2 and MG3 (b)), and YTLH1 and YTLH2 (c)).

131

132

133 Based on the thermal observation at Borehole MG1, 2.6 m (2017) and 1.9 m (2020) in depth were  
134 respectively the maximum and minimum depths of the permafrost table. Combining the data in  
135 Figure 2b and other observational data, the ALT at Borehole MG2 increased from 4.3 m (2012) to  
136 4.8 m (2016), but thinned to 4.2 m (2019) afterwards. The permafrost table at MG3 was located at  
137 2.8 m (2012 and 2013), 4.0 m (2014) and 3.3 m (2015) in depth during the observation period.  
138 Subtle freeze-thaw cycles were observed at 2.0 m in depth in Borehole GH4 (Figure 2a<sub>2</sub>), and the  
139 0 °C isotherms in Figure 3a indicated a range of ALT from 2.2 m (2016) to 2.0 m (2018). In Borehole  
140 GH5, despite of a small temperature range (0.5°C) at the depth of 6.0 m, freeze-thaw cycles took  
141 place. During the monitoring period, the sensor at 7.0 m in depth showed all negative temperatures,  
142 but in the left proximity of 0 °C, all year round, with a multi-year average of mean annual soil  
143 temperature at -0.08°C. The thawing front reached down to the depth of 7.0 m every year (Figure  
144 3b), which means the permafrost table here has been lowered to 7.0 m in depth. In Borehole YTLH1,  
145 ground thaw occurred occasionally at 2.0 m, for an example, in October 2016, but the ALT mostly  
146 varied from 1.5 m (2011) to 1.0 m (2017) during the observation (Figure 3c). In the same period in  
147 2016, -0.1 °C was registered as the highest temperature at 2.0 m in depth in Borehole YTLH2  
148 (Figure 2c<sub>2</sub>), but an above-zero temperature, at 1.5 m depth. The depth of the permafrost table  
149 fluctuated between 1.6 m (2017) and 2.0 m (2011 and 2016) (Figure 3d).

150

151 Figure 3 Variability of 0 °C isotherms (black curves) of ground temperature for Boreholes GH4  
152 (a), GH5 (b), YTLH1 (c), and YTLH2 (d). The empty space indicates the period of missing data.

#### 153 **3.2 Change trends of permafrost temperature at depths**

154 Figure 4 highlights the changes in thermal regimes of permafrost at different depths in Boreholes  
155 MG1, MG2 and MG3. Ground temperature was on the rise, but its amplitude decreased with depth  
156 since the beginning of observation in 2012. In Borehole MG1, the amplitude of ground temperatures  
157 below 8 m in depth was no more than 0.4 °C, and seasonal variability was hardly detectable at



158 depths of 16 and 20 m. The results of linear fitting (red trend lines) indicate an overall warming  
159 trend of permafrost during 2012-2020. A multi-year average of mean annual ground temperature  
160 (MAGT, at 20 m; from 2012 to 2020) of  $-0.8\text{ }^{\circ}\text{C}$  was obtained in Borehole MG1. In Borehole MG2,  
161 ground temperature varied slightly ( $\pm 0.06\text{ }^{\circ}\text{C}$ ) with the seasons even at the depth of 20 m, where the  
162 MAGT was about  $-0.7\text{ }^{\circ}\text{C}$ . Permafrost here was also warming, with a rising amplitude of  $0.1\text{--}0.2\text{ }^{\circ}\text{C}$   
163 from 2012 to 2020. The valid monitoring period was less than 5 years in Borehole MG3 (1 January  
164 2012 to 29 April 2016), when the largest ground temperature range of  $0.2\text{--}0.5\text{ }^{\circ}\text{C}$  was detected  
165 between 8 m and 20 m. Similar to the Borehole MG2, permafrost at 20 m in depth in Borehole MG3  
166 has been experiencing some seasonal variations, with a multi-year average of MAGT at  $-0.9\text{ }^{\circ}\text{C}$ .

167

168 Figure 4. Variability of permafrost temperatures at depths of 8, 10, 12, 16 and 20 m in Boreholes  
169 MG1, MG2 and MG3 in Mangui, northern Da Xing'anling Mountains, Northeast China during  
170 2012-2020. GT stands for ground temperature.

171 Permafrost at depths of 8 and 20 m in Boreholes GH4 and GH5 (Figure 5) warmed by  $1.5\text{--}0.2$   
172 and  $0.2\text{--}0.1\text{ }^{\circ}\text{C}$ , respectively, during 2012-2020. The warming of permafrost at GH5 was  
173 insignificant in comparison with that at other sites. Mean annual soil temperature at 8 m in depth  
174 have slightly warmed from  $-0.17\text{ }^{\circ}\text{C}$  in 2012 to  $-0.16\text{ }^{\circ}\text{C}$  in 2019, and; the MAGT at 20 m in depth,  
175 from  $-0.60$  to  $-0.57\text{ }^{\circ}\text{C}$  over the same period. MAGT at 20 m in depth was averaged at  $-0.59\text{ }^{\circ}\text{C}$   
176 during 2012-2019. However, permafrost at GH4 was relatively cold, with a multi-year average of  
177 MAGT at  $-2.83\text{ }^{\circ}\text{C}$  at 20 m in depth. According to Figure 5, ground temperatures fluctuated  
178 seasonally at above 20 m in depth. However, seasonal variations in ground temperature dwindled  
179 gradually below 30 m (Figure 6), leaving only inter-annual variations. Ground temperatures in  
180 Borehole GH4 increased with increasing depth ( $-2.51$ ,  $-1.76$  and  $-0.41\text{ }^{\circ}\text{C}$  at 30, 50 and 80 m,  
181 respectively), whereas the thermal fluctuations declined downwards ( $0.2\text{ }^{\circ}\text{C}$  at 20 and 30 m in depth,  
182 but  $0.03\text{ }^{\circ}\text{C}$  at 80 m). Thus, during 2012-2020, the ground at depths of 30-80 m at the GH4 site was  
183 warming at an average rate of  $0.004\text{--}0.020\text{ }^{\circ}\text{C}/\text{yr}$ .

184 Figure 5. Variations in permafrost temperatures at depths of 8, 10, 12, 16 and 20 m in Boreholes  
185 GH4 and GH5 in Gen'he, northern Da Xing'anling Mountains, Northeast China during 2012-  
186 2020. GT stands for ground temperature.

187

188 Figure 6. Variability of deep permafrost temperatures at depths of 30 – 80 m for Borehole GH4 in  
189 Gen'he, northern Da Xing'anling Mountains, Northeast China during 2012-2020. GT stands for  
190 ground temperature.

191 In Borehole YTLH2, remarkable seasonal variations were noted at each measured depth. The  
192 seasonal amplitude of ground temperature gradually dampened with increasing depth, varying from  
193 approximately  $0.5\text{ }^{\circ}\text{C}$  at 8 m in depth to less than  $0.1\text{ }^{\circ}\text{C}$  at 20 m. Unlike permafrost in Mangui town  
194 and Gen'he city, a significant cooling of permafrost was detected at all depths except 20 m at  
195 YTLH2 during the 10-year observation (Figure 7). The average rate of temperature change at 20 m  
196 depth is close to  $0\text{ }^{\circ}\text{C}/\text{yr}$  and the MAGT here has been roughly maintained at  $-0.49\text{ }^{\circ}\text{C}$  in the past  
197 decade.

198

199



200 Figure 7. Variability of permafrost temperatures at depths of 8, 12, 16 and 20 m at Borehole  
201 YTLH2 in Yituli'he in northern Da Xing'anling Mountains, Northeast China during 2012-2020.  
202 GT stands for ground temperature.  
203

#### 204 **4 Discussion**

##### 205 *Change trends of near-surface permafrost temperatures*

206 Based on the analysis in Section 3.1, it can be inferred that changes in the ground thermal  
207 regimes of the ecosystem-dominated permafrost on the northwestern slope of the Da Xing'anling  
208 Mountains are mainly controlled by changes in local factors, such as vegetation and snow covers  
209 and human activities, especially in the active layer thickness (ALT). For example, ALT ranges from  
210 2.5 m in 2016 and 2017 to 1.9 m in 2020 for the site in shrubs (MG1), 4.8 m in 2017 to 4.2 m in  
211 2020 in sedge meadow (MG2) and 2.9 m in 2012 to 4.0 m in 2014 in the farmer's backyard (MG3)  
212 during the observation period. Apparently, the Borehole MG1, far away from downtown Mangui,  
213 had the least ALT because of more shading effect of shrubs than that of meadow (MG2) and less  
214 anthropogenic impact than that of backyard (MG3). Declining trend of ALT was also observed in  
215 the Nanwenghe Wetlands Reserve on the southern slope of the Da Xing'anling-Yile'huli Mountain  
216 Knots, Northeast China, probably driven by a rising surface and thermal offsets of vegetation cover  
217 and organic soils (He et al., 2021). Additionally, at the MG3 site, the smaller ALT could be attributed  
218 to the shading effect of the farmer's house and more heat loss to the atmosphere caused by snow  
219 removal in the yard in winter as well. In Gen'he, at the site of Borehole GH4 in a primeval forest,  
220 ALT remained unchanged at 2.2 m from 2012 to 2016 and, without human disturbance, permafrost  
221 was well-preserved. On the contrary, at the GH5 site in the suburb meadow frequently disturbed by  
222 the nearby livestock, a complex thermal regime was observed in the active layer. Ground  
223 temperatures at the depths of 3.5-6.0 m were negative from March to September and positive in  
224 other time every year, and; not until 7.0 m in depth, where it became below 0° C all the year round.  
225 By definition, the active layer is the layer above permafrost that freezes in winter and thaws in  
226 summer. Therefore, 7 m is supposed to be the reasonable ALT or the depth of the permafrost table,  
227 and there might be no supra-permafrost subaerial talik (Jin et al., 2021) between the active layer and  
228 the permafrost table at this site, i.e., attached permafrost. However, the supra-permafrost subaerial  
229 talik, which has appeared in the Nanwenghe Wetlands Reserve about 300 km to the east of the study  
230 site (He et al., 2021), may develop at this site in the future. In Yituli'he, the two boreholes (YTLH1  
231 and YTLH2) are, about 20 m apart, both in the meadowy swamp to the east of the railway and to  
232 the west of highway. Permafrost here is well developed, partially thanks to the sufficient moisture  
233 provided by lowland swamp, which also possibly facilitates the formation of ice wedges (Yang and  
234 Jin, 2011).

235 Notably, there was a decreasing trend in ground temperatures at shallow depths no matter in  
236 summer or winter during 2010-2020 (Figure 2), otherwise suggesting a cooling permafrost at  
237 shallow depths in the last decade on the northwestern slope of the Da Xing'anling Mountains if no  
238 ground-surface conditions are taken into account. This could be related to declining winter  
239 precipitation and snow cover in this area during the observational period. Figure 8b shows a barely  
240 changed mean positive air temperature (MPAT) in Gen'he in the past decade, but winter  
241 precipitation (Figure 8a) and snow cover, including the maximal snow depth (Figure 8c) and snow  
242 duration (Figure 8d), declined slightly, driving the cooling of shallow permafrost in this region. In  
243 addition, the maximum thaw depth (MTD) in Yituli'he was rising but with fluctuations during 1980-



244 2005, but it presented a fluctuating downward trend during 2009-2020 (Figure 9), also implying a  
245 cooling of shallow permafrost.

246

247 Figure 8. Climatic characteristics of Gen'he on the northwestern flank of the northern Da  
248 Xing'anling Mountains in Northeast China in the past ten years

249

250 Figure 9. The maximum thaw depth in Yituli'he on the northwestern flank of the northern Da  
251 Xing'anling Mountains in Northeast China between 1980-2020 (Black squares appeared in the paper  
252 from Jin et al. (2007), red ones are obtained in this observation. The two boreholes are 10 m from each  
253 other, with similar surface, hydrology and soil conditions.)

254 *Change trends of permafrost temperatures at larger depths*

#### 255 **Permafrost in Mangui**

256 During the observation period, the averages of MAGTs at the depth of 20 m were  $-0.79$ ,  $-0.70$   
257 and  $-0.93^{\circ}\text{C}$ , respectively, in shrubs (MG1), meadow (MG2) and farmer's backyard, indicating a  
258 poor correlation between the thermal state of deeper permafrost and vegetation cover or anthropic  
259 disturbances. However, there was a close relationship between permafrost change at larger depths  
260 and land surface conditions. Permafrost below 8 m was significantly warming in the last decade  
261 under a warming climate (Figure 4). In Borehole-MG1 and Borehole-MG2 in particular, the rates  
262 of ground warming increased slightly with depth ( $<0.03^{\circ}\text{C/a}$  for MG1 and  $<0.02^{\circ}\text{C/a}$  for MG2),  
263 demonstrating a less significant thermal rising in deeper permafrost. Within the zone of  
264 discontinuous permafrost, the negative relationship between effective leaf area index ( $\text{LAI}_e$ ) and  
265 soil moisture may contribute to differential rates of permafrost thaw (Baltzer et al., 2014). Therefore,  
266 more effective water uptake by shrubs than meadow results in lower soil moisture, leading to a more  
267 rapid thaw of permafrost at the MG1 site than that at the MG2 site. The warming rate of permafrost  
268 in Borehole MG3, with a large warming range, decreased with depth ( $0.05^{\circ}\text{C/a}$  at depths of 10 and  
269 12 m, but approximately  $0.02^{\circ}\text{C/a}$  at depths of 16 and 20 m), probably due to short monitoring  
270 period and less data. However, it does verify that, in Mangui, permafrost at depths is warming or  
271 degrading in the last decade.

#### 272 **Permafrost in Gen'he**

273 In Borehole GH4, lower ground temperatures and greater warming range was observed in  
274 comparison with those in Borehole GH5 in the last decade (Figure 4). Even at depths of 70 and 80  
275 m, ground temperatures were still rising with time at appreciable warming rates (Figure 5),  
276 reflecting the impact of climatic warming on permafrost at greater depths. A subtle warming trend  
277 of permafrost at depths of 8-20 m in Borehole GH5 was also detected with a rate of  $0.004^{\circ}\text{C/a}$   
278 during the observation period (Figure 4). This warming rate of ground temperature is similar to that  
279 of the Borehole 85-8A in the southern zone of discontinuous permafrost in North America, where  
280 the permafrost is often vertically in isothermal condition and close to  $0^{\circ}\text{C}$  in ground temperature  
281 (Smith et al., 2010). In this situation, latent heat effects are considered as the key factor for leading  
282 to isothermal conditions in the ground and allowing permafrost to persist under a warming climate  
283 (Smith et al., 2010). If the effect of large thermal inertia lasts long enough, the supra-permafrost  
284 subaerial talik will be highly likely to form and permafrost will be gradually buried. In a word,  
285 permafrost degradation in Gen'he is also evident at present in both forested landscape and anthropic



286 zones, particularly in the latter one.

### 287 **Permafrost in Yituli'he**

288 According to previous study (Jin et al., 2007), MAGT at 13 m in Yituli'he rose by 0.2 °C during  
289 1984-1997, continuously rising from -1.00 °C in 1997 to -0.55 °C in 2010, except during the short  
290 suspension of monitoring (2005-2008), and peaking at -0.53 °C in 2013. After that, it kept lowering  
291 consecutively and by 2018 it was lower than -0.70 °C, showing an evident cooling trend of  
292 permafrost in a sharp contrast to the ground warming trends in Gen'he, Mangui, and other  
293 permafrost regions in the world (Douglas et al., 2021; Farquharson et al., 2019). Based on the  
294 investigation, there was once a Railway Branch Administration in Yituli'he town since 1964s to  
295 1970s, with a population of over 30,000, but the branch was terminated in 1998. After that, more  
296 and more people emigrated and less than 10,000 residents have remained at present, thus leaving a  
297 chance for restoration of the local eco-environment and for recovering permafrost temperature.

298 So far, the mitigation of permafrost degradation becomes considerably difficult in the context of  
299 a persistent climate warming (Brown et al., 2015; Luo et al., 2018). However, within the dried  
300 margin of the Twelvemile Lake (66°27'N, 145°34'W), permafrost aggradation has taken place due  
301 to willow shrub uptake of summer recharge and summer shading recharge reduction (Briggs et al.,  
302 2014). Beer et al. (Beer et al., 2020) also found that most permafrost-affected soil could be preserved  
303 by increasing the population density of big herbivores in northern high-latitude ecosystems as a  
304 result of reducing insulation of winter snow cover. The fact that permafrost is cooling in Yituli'he  
305 demonstrates that the ecosystem-protected permafrost in discontinuous permafrost zone may  
306 recover if the disturbances, such as human activities, dwindle. Thus, our research results would  
307 provide key evidence for the preservation of permafrost in areas with intense past anthropic  
308 disturbances (Serban et al., 2021).

### 309 **5 Conclusions**

310 Long-term records of permafrost monitoring presented here from the northwestern flank of the Da  
311 Xing'anling Mountains in Northeast China show some important characteristics of ground thermal  
312 regimes in the past eight years (2012-2020). The lowest MAGT at 20 m in depth was -2.83 °C in  
313 Borehole GH4 in a primeval larch forest, and -0.94, -0.80, -0.70, -0.60 and -0.49 °C, respectively,  
314 at MG3, MG1, MG2, GH5 and YTLH2. The maximum of the burial depth of the permafrost table  
315 at about 7.0 m was discovered in Borehole GH5, and the minimum, 1.1 ~ 1.5 m at YTLH1. The  
316 permafrost table was at depths of about 2.0 m at GH4 and YTLH2, and 2.5, 5.0 and 4.0 m at MG1,  
317 MG2 and MG3, respectively. Local factors, such as vegetation and snow covers and human  
318 activities, are supposed to be mainly responsible for the changes in the ALT and the thermal state of  
319 shallow permafrost in the study area. The most important fact is that ground cooling at shallow  
320 depths, as well as the declining ALT in Yituli'he after 2009, has been detected during the observation  
321 period, which is probably caused by fairly constant MPAT (mean positive air temperature) and  
322 weakened insulation of winter snow cover.

323 Apart from Yituli'he, permafrost warming at large depths was particularly pronounced during the  
324 observation period, even at depths of 70 and 80 m, with different ground warming rates. It is  
325 noteworthy that geothermal gradient at depths in Borehole GH5 is almost zero (vertically no change)  
326 and with MAGT at about 0 °C due to huge thermal inertia of the ice-rich permafrost. This may most  
327 likely lead to the formation of the supra-permafrost subaerial talik soon. At the Yituli'he Permafrost





328 Observatory, permafrost has been cooling since the re-establishment of monitoring program in 2010;  
329 the rapidly declining local population might have relieved its stress on the eco-environment and  
330 resulted in permafrost recovery. This fact makes it possible to mitigate the permafrost degradation in  
331 in the zone of ecosystem-dominated permafrost, offering a new thought for permafrost protection.

### 332 **Author Contributions**

333 XC, HJ, and RH designed the study. XC wrote the manuscript and performed the analysis. YZ  
334 plotted the figures. XL, XJ and GL contributed parts of the field data. HJ improved the writing and  
335 structure of the paper.

### 336 **Competing interests**

337 The contact author has declared that neither they nor their co-authors have any competing interests.

### 338 **Disclaimer**

339 Publisher's note: Copernicus Publications remains neutral with regard to jurisdictional claims in  
340 published maps and institutional affiliations.

### 341 **Special issue statement**

342 This article is part of the special issue "Extreme environment datasets for the three poles". It is not  
343 associated with a conference.

### 344 **Acknowledgements**

345 Thanks go to the Inner Mongolia Agricultural University for fieldwork support and the Gen'he  
346 Weather Bureau for meteorological data provision. This study was financially supported by the  
347 National Natural Science Foundation of China (Grant Nos. 41971079, 41671059, 41871052 and  
348 U20A2082) and the Natural Science Program of Hunan Province (Grant No. 2020JJ5161).

### 349 **Data availability**

350 Chang, X.: Geotemperature observation data set of Genhe River (2012-2019), National Tibetan  
351 Plateau Data Center [data set], DOI: 10.11888/Geocry.tpd.271752, 2021.

### 352 **Reference**

- 353 Baltzer, J. L., Veness, T., Chasmer, L. E., Sniderhan, A. E., and Quinton, W. L.: Forests on thawing  
354 permafrost: fragmentation, edge effects, and net forest loss, *Global change biology*, 20, 824-834,  
355 10.1111/gcb.12349, 2014.  
356 Beer, C., Zimov, N., Olofsson, J., Porada, P., and Zimov, S.: Protection of Permafrost Soils from Thawing  
357 by Increasing Herbivore Density, *Scientific reports*, 10, 4170, 10.1038/s41598-020-60938-y, 2020.



- 358 Biskaborn, B. K., Smith, S. L., Noetzi, J., Matthes, H., Vieira, G., Streletskiy, D. A., Schoeneich, P.,  
359 Romanovsky, V. E., Lewkowicz, A. G., Abramov, A., Allard, M., Boike, J., Cable, W. L., Christiansen,  
360 H. H., Delaloye, R., Diekmann, B., Drozdov, D., Eitzelmüller, B., Grosse, G., Guglielmin, M., Ingeman-  
361 Nielsen, T., Isaksen, K., Ishikawa, M., Johansson, M., Johannsson, H., Joo, A., Kaverin, D., Kholodov,  
362 A., Konstantinov, P., Kröger, T., Lambiel, C., Lanckman, J.-P., Luo, D., Malkova, G., Meiklejohn, I.,  
363 Moskalenko, N., Oliva, M., Phillips, M., Ramos, M., Sannel, A. B. K., Sergeev, D., Seybold, C., Skryabin,  
364 P., Vasiliev, A., Wu, Q., Yoshikawa, K., Zheleznyak, M., and Lantuit, H.: Permafrost is warming at a  
365 global scale, *Nature Communications*, 10, 264, [10.1038/s41467-018-08240-4](https://doi.org/10.1038/s41467-018-08240-4), 2019.
- 366 Briggs, M. A., Walvoord, M. A., McKenzie, J. M., Voss, C. I., Day-Lewis, F. D., and Lane, J. W.: New  
367 permafrost is forming around shrinking Arctic lakes, but will it last?, *Geophysical Research Letters*, 41,  
368 1585-1592, <https://doi.org/10.1002/2014GL059251>, 2014.
- 369 Brown, D. R. N., Jorgenson, M. T., Douglas, T. A., Romanovsky, V. E., Kielland, K., Hiemstra, C.,  
370 Euskirchen, E. S., and Ruess, R. W.: Interactive effects of wildfire and climate on permafrost degradation  
371 in Alaskan lowland forests, *Journal of Geophysical Research: Biogeosciences*, 120, 1619-1637,  
372 <https://doi.org/10.1002/2015JG003033>, 2015.
- 373 Brown, J., Hinkel, K. M., and Nelson, F. E.: The circumpolar active layer monitoring (calm) program:  
374 Research designs and initial results, *Polar Geography*, 24, 166-258, [10.1080/10889370009377698](https://doi.org/10.1080/10889370009377698), 2000.
- 375 Douglas, T. A., Hiemstra, C. A., Anderson, J. E., Barbato, R. A., Bjella, K. L., Deeb, E. J., Gelvin, A. B.,  
376 Nelsen, P. E., Newman, S. D., Saari, S. P., and Wagner, A. M.: Recent degradation of interior Alaska  
377 permafrost mapped with ground surveys, geophysics, deep drilling, and repeat airborne lidar, *The*  
378 *Cryosphere*, 15, 3555-3575, [10.5194/tc-15-3555-2021](https://doi.org/10.5194/tc-15-3555-2021), 2021.
- 379 Farquharson, L. M., Romanovsky, V. E., Cable, W. L., Walker, D. A., Kokelj, S. V., and Nicolsky, D.:  
380 Climate Change Drives Widespread and Rapid Thermokarst Development in Very Cold Permafrost in  
381 the Canadian High Arctic, *Geophysical Research Letters*, 46, 6681-6689,  
382 <https://doi.org/10.1029/2019GL082187>, 2019.
- 383 Grebenets, V. I., Tolmanov, V. A., and Streletskiy, D. A.: Active Layer Dynamics Near Norilsk, Taimyr  
384 Peninsula, Russia, *Geography, Environment, Sustainability*, 14, 55-66, [10.24057/2071-9388-2021-073](https://doi.org/10.24057/2071-9388-2021-073),  
385 2021.
- 386 Gruber, S.: Derivation and analysis of a high-resolution estimate of global permafrost zonation, *The*  
387 *Cryosphere*, 6, [10.5194/tc-6-221-2012](https://doi.org/10.5194/tc-6-221-2012), 2012.
- 388 Guglielmin, M.: Ground surface temperature (GST), active layer and permafrost monitoring in  
389 continental Antarctica, *Permafrost and Periglacial Processes*, 17, 133-143,  
390 <https://doi.org/10.1002/ppp.553>, 2006.
- 391 Guglielmin, M., Worland, M. R., and Cannone, N.: Spatial and temporal variability of ground surface  
392 temperature and active layer thickness at the margin of maritime Antarctica, Signy Island,  
393 *Geomorphology*, 155-156, 20-33, <https://doi.org/10.1016/j.geomorph.2011.12.016>, 2012.
- 394 Guo, W., Liu, H., Anenkhonov, O. A., Shanguan, H., Sandanov, D. V., Korolyuk, A. Y., Hu, G., and Wu,  
395 X.: Vegetation can strongly regulate permafrost degradation at its southern edge through changing  
396 surface freeze-thaw processes, *Agricultural and Forest Meteorology*, 252, 10-17,  
397 <https://doi.org/10.1016/j.agrformet.2018.01.010>, 2018.
- 398 He, R.-X., Jin, H.-J., Luo, D.-L., Li, X.-Y., Zhou, C.-F., Jia, N., Jin, X.-Y., Li, X.-Y., Che, T., Yang, X.,  
399 Wang, L.-Z., Li, W.-H., Wei, C.-L., Chang, X.-L., and Yu, S.-P.: Permafrost changes in the Nanwenghe  
400 Wetlands Reserve on the southern slope of the Da Xing'anling–Yile'huli mountains, Northeast China,  
401 *Advances in Climate Change Research*, 12, 696-709, <https://doi.org/10.1016/j.accre.2021.06.007>, 2021.

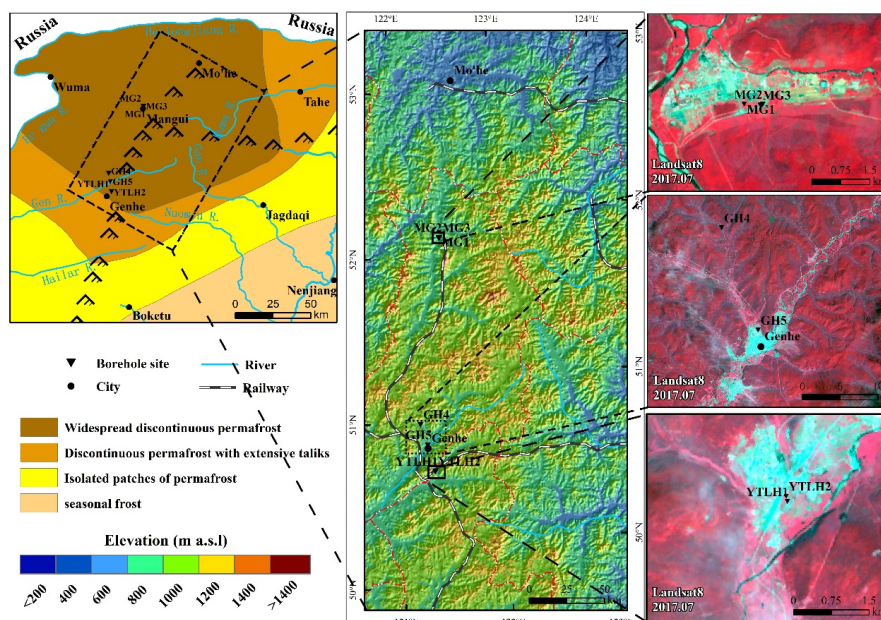


- 402 Hrbáček, F., Vieira, G., Oliva, M., Balks, M., Guglielmin, M., de Pablo, M. Á., Molina, A., Ramos, M.,  
403 Goyanes, G., Meiklejohn, I., Abramov, A., Demidov, N., Fedorov-Davydov, D., Lupachev, A., Rivkina,  
404 E., Láska, K., Kňázková, M., Nývlt, D., Raffi, R., Strelin, J., Sone, T., Fukui, K., Dolgikh, A., Zazovskaya,  
405 E., Mergelov, N., Osokin, N., and Miamin, V.: Active layer monitoring in Antarctica: an overview of  
406 results from 2006 to 2015, *Polar Geography*, 44, 217-231, 10.1080/1088937X.2017.1420105, 2021.
- 407 Jin, H., Wu, Q., and Romanovsky, V.: Degrading permafrost and its impacts, *Advances in Climate*  
408 *Change Research*, 12, 10.1016/j.accre.2021.01.007, 2021.
- 409 Jin, H., Li, S., Cheng, G., Shaoling, W., and Li, X.: Permafrost and climatic change in China, *Global and*  
410 *Planetary Change*, 26, 387-404, [https://doi.org/10.1016/S0921-8181\(00\)00051-5](https://doi.org/10.1016/S0921-8181(00)00051-5), 2000.
- 411 Jin, H., Yu, Q., Lü, L., Guo, D., He, R., Yu, S.-p., Sun, G., and Li, Y.: Degradation of permafrost in the  
412 Xing'anling Mountains, northeastern China, *Permafrost and Periglacial Processes*, 18, 245-258, 2007.
- 413 Li, X.-Y., Jin, H.-J., Wang, H.-W., Marchenko, S. S., Shan, W., Luo, D.-L., He, R.-X., Spektor, V., Huang,  
414 Y.-D., Li, X.-Y., and Jia, N.: Influences of forest fires on the permafrost environment: A review, *Advances*  
415 *in Climate Change Research*, 12, 48-65, <https://doi.org/10.1016/j.accre.2021.01.001>, 2021.
- 416 Li, X., Jin, H., He, R., Huang, Y., Wang, H., Luo, D., Jin, X., Lü, L., Wang, L., Li, W. h., Wei, C., Chang,  
417 X., Yang, S., and Yu, S.: Effects of forest fires on the permafrost environment in the northern Da  
418 Xing'anling (Hinggan) mountains, Northeast China, *Permafrost and Periglacial Processes*, 30, 163-177,  
419 <https://doi.org/10.1002/ppp.2001>, 2019.
- 420 Luo, L., Ma, W., Zhuang, Y., Zhang, Y., Yi, S., Xu, J., Long, Y., Ma, D., and Zhang, Z.: The impacts of  
421 climate change and human activities on alpine vegetation and permafrost in the Qinghai-Tibet  
422 Engineering Corridor, *Ecological Indicators*, 93, 24-35, <https://doi.org/10.1016/j.ecolind.2018.04.067>,  
423 2018.
- 424 Romanovsky, V. E., Smith, S. L., and Christiansen, H. H.: Permafrost thermal state in the polar Northern  
425 Hemisphere during the international polar year 2007–2009: a synthesis, *Permafrost and Periglacial*  
426 *Processes*, 21, 106-116, <https://doi.org/10.1002/ppp.689>, 2010.
- 427 Serban, R., Serban, M., He, R., Jin, H., Yan, L., Xinyu, L., Wang, X., and Li, G.: 46-Year (1973–2019)  
428 Permafrost Landscape Changes in the Hala Basin, Northeast China Using Machine Learning and Object-  
429 Oriented Classification, *Remote Sensing*, 13, 1910, 10.3390/rs13101910, 2021.
- 430 ShanShan Chen, S. Z., Li Sun: Characteristics of permafrost degradation in Northeast China and its  
431 ecological effects: A review, *Sciences in Cold and Arid Regions*, 12, 1-11,  
432 10.3724/sp.j.1226.2020.00001., 2020.
- 433 Shiklomanov, N., Streletskiy, D., and Nelson, F.: Northern Hemisphere Component of the Global  
434 Circumpolar Active Layer Monitoring (CALM) Program, 2012.
- 435 Shur, Y. and Jorgenson, M.: Patterns of Permafrost Formation and Degradation in Relation to Climate  
436 and Ecosystems, *Permafrost and Periglacial Processes*, 18, 7-19, 10.1002/ppp.582, 2007.
- 437 Sim, T. G., Swindles, G. T., Morris, P. J., Baird, A. J., Cooper, C. L., Gallego-Sala, A. V., Charman, D.  
438 J., Roland, T. P., Borken, W., Mullan, D. J., Aquino-López, M. A., and Gałka, M.: Divergent responses  
439 of permafrost peatlands to recent climate change, *Environmental Research Letters*, 16, 034001,  
440 10.1088/1748-9326/abe00b, 2021.
- 441 Smith, S. L., Romanovsky, V. E., Lewkowicz, A. G., Burn, C. R., Allard, M., Clow, G. D., Yoshikawa,  
442 K., and Throop, J.: Thermal state of permafrost in North America: a contribution to the international  
443 polar year, *Permafrost and Periglacial Processes*, 21, 117-135, <https://doi.org/10.1002/ppp.690>, 2010.
- 444 Wei, Z., Jin, H., Zhang, J., Yu, S., Han, X., Ji, Y., He, R., and Chang, X.: Prediction of permafrost changes  
445 in Northeastern China under a changing climate, *Science China Earth Sciences*, 54, 924-935,



446 10.1007/s11430-010-4109-6, 2011.  
447 Yang, S. and Jin, H.:  $\delta^{18}\text{O}$  and  $\delta\text{D}$  records of inactive ice wedge in Yitulihe, Northeastern China and  
448 their paleoclimatic implications, *Science China Earth Sciences*, 54, 119-126, 10.1007/s11430-010-4029-  
449 5, 2011.  
450 Youhua, R., Cheng, G., Zhang, T., Wu, Q., Jin, H., and Jin, R.: Distribution of Permafrost in China: An  
451 Overview of Existing Permafrost Maps, *Permafrost and Periglacial Processes*, 23, 322-333,  
452 10.1002/ppp.1756, 2012.  
453 Zhang, G., Nan, Z., Wu, X., Ji, H., and Zhao, S.: The Role of Winter Warming in Permafrost Change  
454 Over the Qinghai-Tibet Plateau, *Geophysical Research Letters*, 46, 11261-11269,  
455 <https://doi.org/10.1029/2019GL084292>, 2019.  
456 Zhang, T., Nelson, F., and Gruber, S.: Introduction to special section: Permafrost and Seasonally Frozen  
457 Ground Under a Changing Climate, *Journal of Geophysical Research*, 112, 10.1029/2007JF000821, 2007.  
458 Zhang, Z.-Q., Wu, Q.-B., Hou, M.-T., Tai, B.-W., and An, Y.-K.: Permafrost change in Northeast China  
459 in the 1950s–2010s, *Advances in Climate Change Research*, 12, 18-28,  
460 <https://doi.org/10.1016/j.accr.2021.01.006>, 2021.  
461 Zhang, Z., Wu, Q., Xun, X., Wang, B., and Wang, X.: Climate change and the distribution of frozen soil  
462 in 1980–2010 in northern northeast China, *Quaternary International*, 467, 230-241,  
463 <https://doi.org/10.1016/j.quaint.2018.01.015>, 2018.

465



466  
467 Figure 1. Location of the study area and the distribution of borehole sites in the zones of frozen ground in the  
468 northern Da Xing'anling Mountains, Northeast China  
469

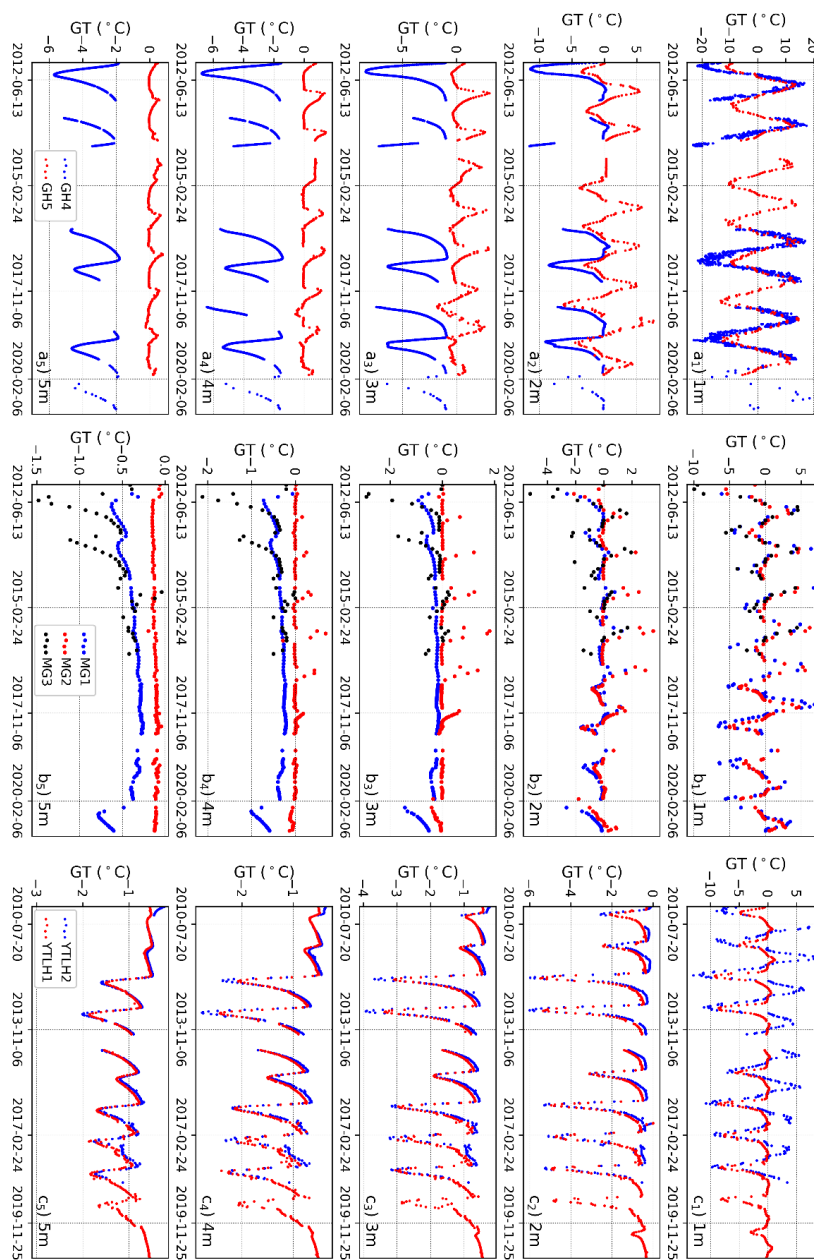


Figure 2. Variability of measured ground temperatures at depths of 1-5 m for Boreholes GH4 and GH5 (a), MG1, MG2 and MG3 (b), and YTLH1 and YTLH2 (c).

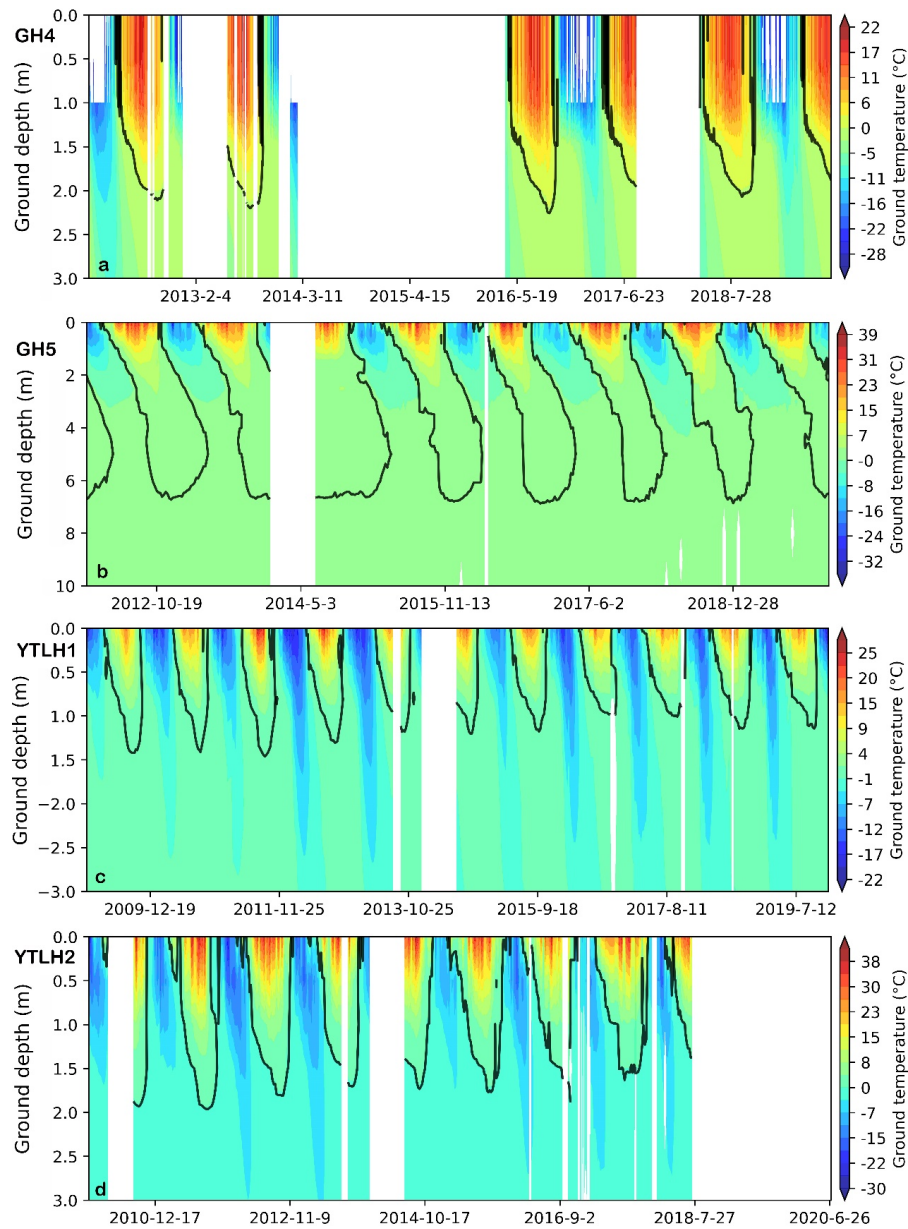


Figure 3 Variability of 0 °C isotherms (black curves) of ground temperature for Boreholes GH4 (a), GH5 (b), YTLH1 (c), and YTLH2 (d). The empty space indicates the period of missing data.

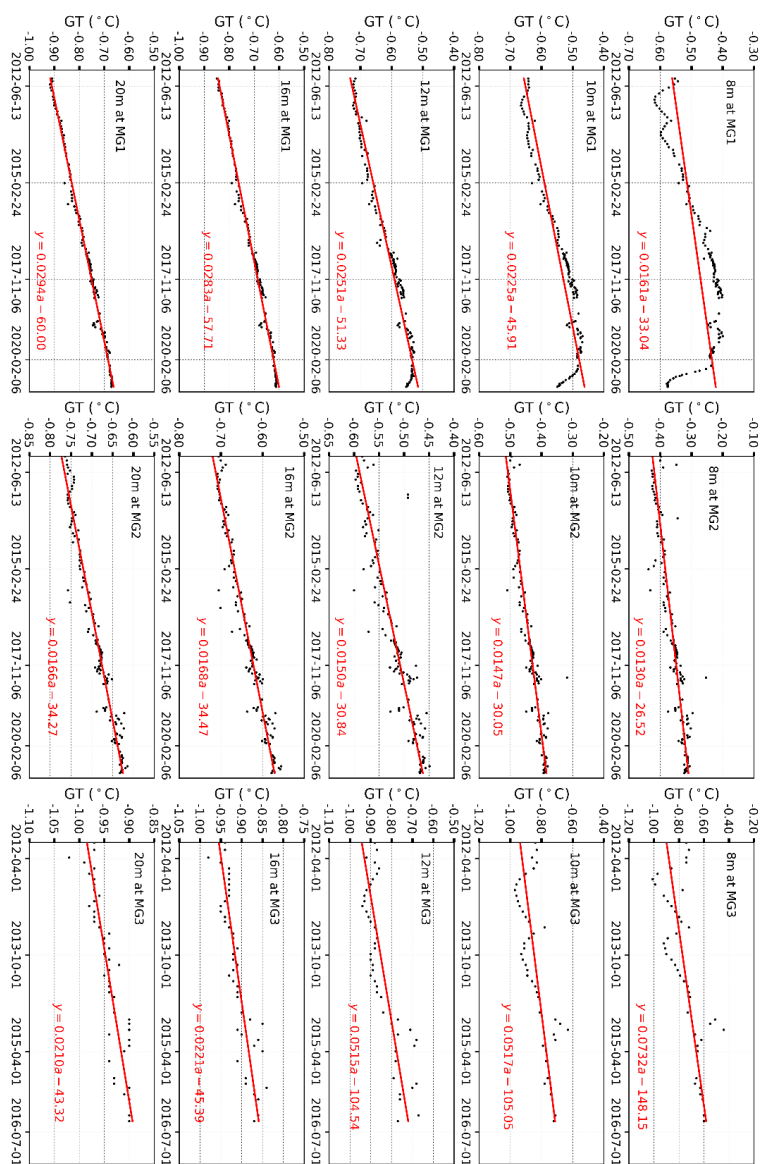


Figure 4. Variability of permafrost temperatures at depths of 8, 10, 12, 16 and 20 m in Boreholes MG1, MG2 and MG3 in Mangui, northern Da Xing'anling Mountains, Northeast China during 2012–2020. GT stands for ground temperature.

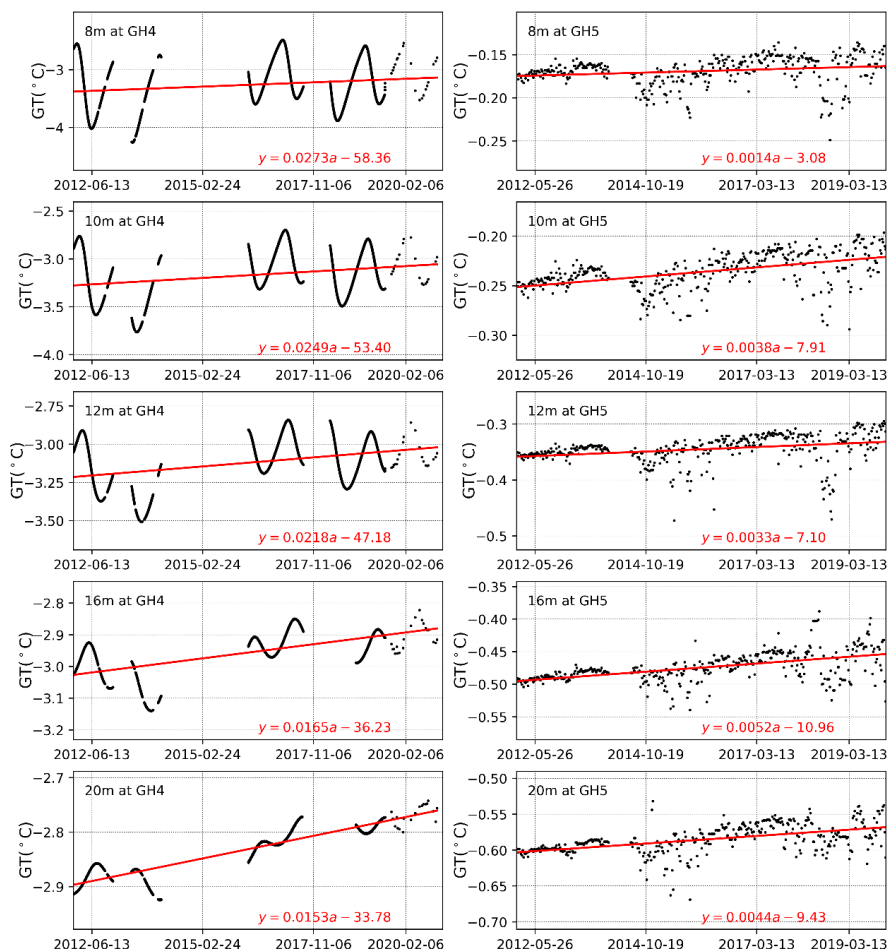


Figure 5. Variations in permafrost temperatures at depths of 8, 10, 12, 16 and 20 m in Boreholes GH4 and GH5 in Gen'he, northern Da Xing'anling Mountains, Northeast China during 2012-2020. GT stands for ground temperature.



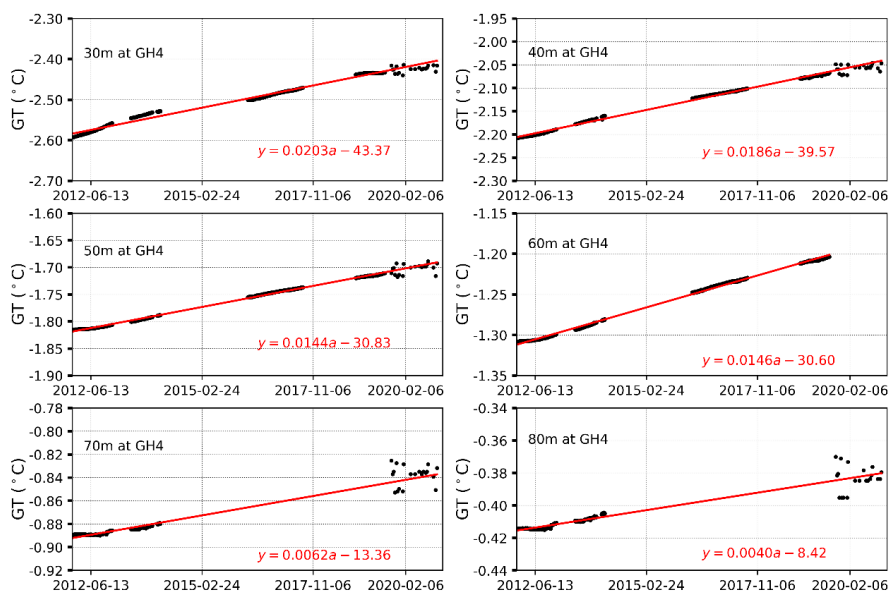


Figure 6. Variability of deep permafrost temperatures at depths of 30 – 80 m for Borehole GH4 in Gen’he, northern Da Xing’anling Mountains, Northeast China during 2012–2020. GT stands for ground temperature.

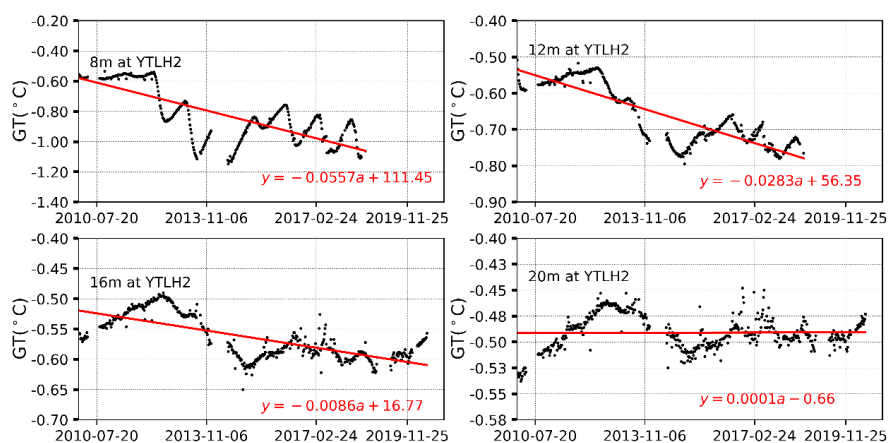


Figure 7. Variability of permafrost temperatures at depths of 8, 12, 16 and 20 m at Borehole YTLH2 in Yituli’he in northern Da Xing’anling Mountains, Northeast China during 2012–2020. GT stands for ground temperature.

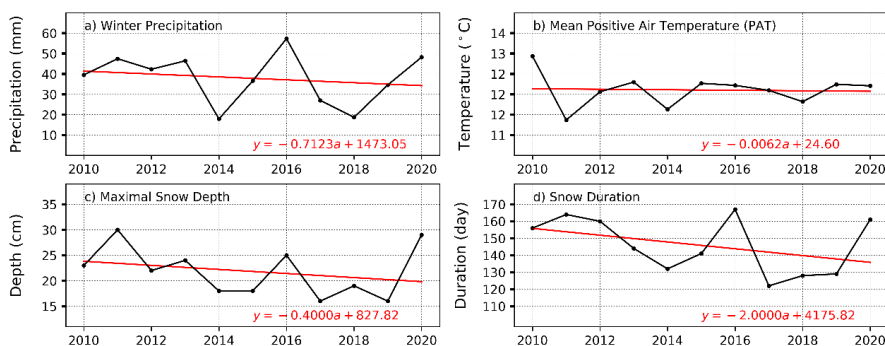


Figure 8. Climatic characteristics of Gen'he on the northwestern flank of the northern Da Xing'anling Mountains in Northeast China in the past ten years

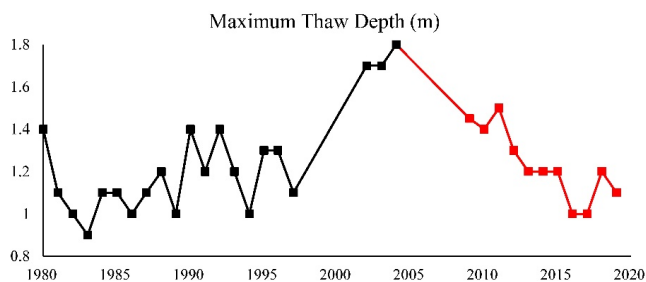


Figure 9. The maximum thaw depth in Yituli'he on the northwestern flank of the northern Da Xing'anling Mountains in Northeast China between 1980-2020 (Black squares appeared in the paper from Jin et al. (2007), red ones are obtained in this observation. The two boreholes are 10 m from each other, with similar surface, hydrology and soil conditions.)



Table 1. Characteristics and monitoring information of ground temperature boreholes in the northwestern part of Da Xing'anling Mountains, Northeastern China

Borehole No.	Lat. (°N)	Long. (°E)	Elev. (m a. s. l.)	Vegetation	Monitoring depths (m)	Time period	Monitoring frequency
MG1	52.037	122.069	633	<i>Betula fruticosa</i> shrubs	0.0, 1.0, 1.5, 2.0, 2.5, 3.0, 3.5, 4.0, 4.5,	2012-2020	Monthly
MG2	52.036	122.075	642	<i>Carex lato</i> meadow	5.0, 6.0, 7.0, 8.0, 9.0, 10.0, 11, 12, 13, 14, 15, 16, 17, 18, 19, 20	2012-2020	Monthly
MG3	52.036	122.076	639	Open courtyard	15, 16, 17, 18, 19, 20	2012-2015	Monthly
GH4	50.932	121.502	811	<i>Betula fruticosa</i> <i>Larix gmelini</i> forest	0.0, 1.0, 1.5, 2.0, 2.5, 3.0, 3.5, 4.0, 4.5, 5.0, 6.0, 7.0, 8.0, 9.0, 10.0, 11, 12, 13, 14, 15, 16, 17, 18, 19, 20, 25, 30, 35, 40, 45, 50, 60, 70, 80	2012-2014, 2016-2017, 2019-2020	Hourly
GH5	50.799	121.530	728	<i>Carex lato</i> meadow	0.0, 1.0, 1.5, 2.0, 2.5, 3.0, 3.5, 4.0, 4.5, 5.0, 6.0, 7.0, 8.0, 9.0, 10.0, 11, 12, 13, 14, 15, 16, 17, 18, 19, 20	2012-2019	Hourly
YT1	50.629	121.549	721	<i>Carex lato</i> swamp	0.0, 0.1, 0.2, 0.5, 0.8, 1.0, 1.6, 2.0, 3.0, 4.0, 5.0, 6.0, 7.0, 8, 15	2009-2019	Weekly
YT2	50.630	121.549	725	<i>Carex lato</i> swamp	0.0, 1.0, 1.5, 2.0, 2.5, 3.0, 3.5, 4.0, 4.5, 5.0, 6.0, 7.0, 8.0, 9.0, 10.0, 11, 12, 13, 14, 15, 16, 17, 18, 19, 20	2010-2017	Weekly